Journal of Coordination Chemistry, 2014
Vol. 67, No. 2, 286–299, http://dx.doi.org/10.1080/00958972.2014.880426

Taylor & Francis
Taylor & Francis Group

Synthesis, characterization, X-ray crystallography, and antimicrobial activities of Ni(II) and Cu(II) complexes with a salicylaldehyde-based thiosemicarbazone ligand

NITIS CHANDRA SAHA*†, RAJESH PRADHAN†, MOUSUMI DAS‡, NASIMA KHATUN‡, DEBMALYA MITRA‡, AMALESH SAMANTA‡, ALEXANDRA M.Z. SLAWIN§, ATISH DIPANKAR JANA¶, JULIA KLANKE‖ and EVA RENTSCHLER‖

†Department of Chemistry, University of Kalyani, Nadia, India
‡Division of Microbiology, Department of Pharmaceutical Technology, Jadavpur University, Kolkata, India
§School of Chemistry, University of St Andrews, Fife, UK
¶Department of Physics, Behala College, Kolkata, India
‖Institute of Inorganic and Analytical Chemistry, Johannes Gutenberg University, Mainz, Germany

(*Received 9 October 2013; accepted 5 December 2013*)

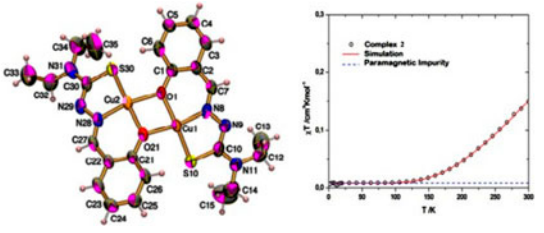

A new salicylaldehyde-based 'ONS' tridentate salicylaldehyde-N(4)-diethylthiosemicarbazone (H_2SANEt_2) has been synthesized and characterized by elemental analyses, mass, IR, and ^1H NMR spectral parameters. The coordination mode of the synthesized ligand is reported by solid state isolation and physico-chemical identification of Ni(II) and Cu(II) complexes, $[Ni(SANEt_2)]_2$ (**1**) and $[Cu(SANEt_2)]_2$ (**2**). Both complexes are neutral and oxygen-bridged dinuclear species. The ligand is bideprotonated 'ONS' tridentate in both complexes. IR spectral data indicate that coordination of each metal of the two complexes occurs through phenolic oxygen, azomethine nitrogen, and thiolato sulfur. X-ray crystallographic data of **1** and **2** (both monoclinic, $P2_1/c$) show a MONSO (where M=Ni and Cu) square-planar coordination around each metal. Magnetic studies of **2** show that the two Cu(II) centers are strongly antiferromagnetically coupled via the bridging phenoxo O. All the synthesized compounds were tested for their *in vitro* antimicrobial activities against pathogenic bacteria. The inhibition power of the complexes was greater than the parent ligand.

Keywords: Thiosemicarbazone; Ni, Cu-complexes; Crystal structures; Magnetic property; Antimicrobial activity

*Corresponding author. Email: nitissaha@klyuniv.ac.in

1. Introduction

Thiosemicarbazones are an excellent class of nitrogen & sulfur containing ligands with interesting bonding capabilities, biological and chemical properties [1]. Presence of sulfur in these complexes often shows various pharmacological activities [2] including antitumoral [3–7], anticancer [8], antibacterial [9], antifungal [10], and antiHIV [11] activity. The chemical nature of the moiety attached to the C=S carbon in thiosemicarbazone derivative is responsible for various biological and medicinal properties. Derivatives of thiosemicarbazones inhibit the activities of ribonucleotide reductase [12]. Because of their biological potency, there is interest in metal complexes of heterocyclic thiosemicarbazones as well as salicylaldehyde-thiosemicarbazones. Deprotonation of phenoxy hydrogen and N3 hydrogen of the ligand form dianionic compound that coordinates with various metal via phenoxy oxygen, imine nitrogen, and thiolate sulfur [13]. Dinuclear copper(II) complexes of Schiff-based ligands have interesting properties as well as applications in magnetism, catalysis, biology, etc. Deprotonation of phenoxy and bridging oxygen with two metals makes the salicylaldehyde-thiosemicarbazone a potential dinucleating ligand. Hydroxo-and phenoxo-bridged metal complexes involving M_2O_2 (M=Ni(II), Cu(II), etc.) bridging present in various metallo-enzymes have importance in biochemistry [14].

As part of our efforts towards synthesis and characterization of new metal ion materials containing bio-relevant thiosemicarbazones and in continuation of our earlier publication [15], this communication reports the synthesis, spectroscopic and structural characterization, and antimicrobial activities of Ni(II) and Cu(II) complexes with H_2SANEt_2 along with the magnetic properties of the Cu(II) complex.

2. Experimental setup

2.1. *Materials and measurements*

Mueller-Hinton agar was purchased from Merck India Ltd. All other reagents were of AR grade and obtained from commercial sources and used without purification. Spectrograde solvents were used for spectral measurements. Elemental analyses (C, H, N, and S) were done with a Perkin-Elmer 2400 CHNS/O analyzer. The nickel and copper contents of the complexes were determined gravimetrically as anhydrous dimethylglyoximatonickel(II) and iodometrically, respectively. Electronic spectra were recorded on a Shimadzu UV-2401PC spectrophotometer. IR spectra were recorded (4000–450 cm^{-1}) on a Perkin-Elmer L120-000A FT-IR spectrophotometer with KBr pellets. ^1H NMR spectrum of the ligand was recorded in DMSO-d_6 with a Bruker AC 400 superconducting FT NMR. Mass spectroscopy was performed with a Jeol JMS-D300 mass spectrometer. A Rigaku Mercury 70 diffractometer was used to collect X-ray data of the complexes. Antiferromagnetism of the complex was performed with SQUID magnetometer MPMS-7 Quantum Design.

2.2. *Synthesis*

2.2.1. Synthesis of H_2SANEt_2. Salicylaldehyde-N(4)-diethylthiosemicarbazone, H_2SANEt_2, (figure 1) was synthesized by refluxing an equimolar mixture of S-methyldithiocarbazate [16] and salicylaldehyde in dry ethanol involving conversion of salicylaldehyde into

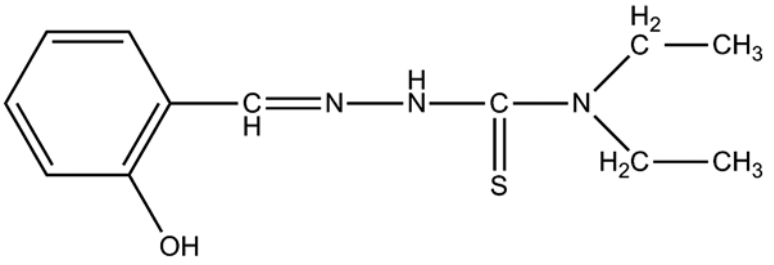

Figure 1. Formulation of H_2SANEt_2.

its S-methyldithiocarbazate derivative, followed by transamination [17] of the derivative with diethylamine. An orange microcrystalline solid (from ethanol) was obtained with a yield of *ca.* 70–75% (m.p.: 103–104 °C). Anal. Calcd for $C_{12}H_{17}N_3OS$ (%): C, 57.34; H, 6.82; N, 16.70; S, 12.74. Found (%): C, 56.75; H, 5.93; N, 16.08; S, 12.21. *m/z*: 252.04 (M^+, 98%).

2.2.2. Synthesis of $[Ni(SANEt_2)]_2$ (1) and $[Cu(SANEt_2)]_2$ (2). The Ni(II) and Cu(II) complexes were prepared by refluxing ethanolic solutions of the ligand (1.05 mM) and Ni $(OAc)_2$ or $Cu(OAc)_2$ (1.05 mM) in a water bath for 2 h. Bright yellow ligand solution, in both the cases, was changed to dark brown. On slow evaporation of the dark brown solutions, the desired Ni(II) or Cu(II) complexes crystallized, and then were filtered off, washed with cold ethanol, and were dried over anhydrous $CaCl_2$; the yield varied between 70 and 77%. Dark brown needle-shaped single crystals, in both the cases, were obtained from pentane/dichloromethane mixture suitable for X-ray diffraction. Anal. Calcd for $C_{24}H_{30}N_6Ni_2O_2S_2$ (%): C, 46.80; H, 4.91; N, 13.64; S, 10.40; Ni, 19.06. Found: C, 46.20; H, 4.08; N, 12.98; S, 10.12; Ni, 18.80. *m/z*: 614.99 (M^+, 44%). Anal. Calcd for $C_{24}H_{30}N_6Cu_2O_2S_2$ (%): C, 46.05; H, 4.83; N, 13.43; S, 10.23; Cu, 20.32. Found: C, 45.80; H, 4.08; N, 12.98; S, 10.01; Cu, 19.80. *m/z*: 624.90 (M^+, 56%).

2.3. *Single-crystal X-ray diffraction studies*

X-ray diffraction data of $[Ni(SANEt_2)]_2$ (**1**) and $[Cu(SANEt_2)]_2$ (**2**) were collected on a Rigaku Mercury 70 diffractometer. The radiation used was MoK_α and the data were corrected for Lorentz-polarization and absorption effects. The structures were solved by Patterson Methods (DIRDIF99 PATTY) and refined using full-matrix least squares based on $/F_{obs}/^2$ [18]. The non-hydrogen atoms were refined anisotropically, while hydrogens, either located from difference electron density maps or generated using idealized geometry, were used in the structure factor calculations with isotropic thermal parameters using the "riding" model. Neutral atom scattering factors [19] were used and anomalous dispersion effects were included in F_{Calcd} [20].

2.4. *DFT calculation*

In order to obtain the optimized geometry of the complex species, a representative DFT calculation was carried out taking the dinuclear Ni(II) complex, with *B3LYP* density functional and *6-31G(d,p)* basis set using GAMESS software package [21].

2.5. *Antimicrobial activity*

The compounds were tested for their *in vitro* antimicrobial activities using 18 types of microorganisms, *Escherichia coli* 55/10HD, *Micrococcus luteus* 9341, *Salmonella typhi* 74, *Staphylococcus aureus* ML191, *Klebsiella pneumoniae* 714, *Pseudomonas* AMRI 100, *Vibrio cholerae* 1363175, *Shigella sonnei* BCH217, *Proteus vulgaris* 24, *Streptococcus faecalis* 52, *Shigella dysenteriae* 1, *Bacillus cereus* 11778, *Streptococcus epidermidis* 12228 (both Gram-positive and negative), *Pseudomonas aeruginosa* 25619, *Micrococcus sp.* 10240, *Bacillus subtilis* 6633, *Bacillus pumilus* 14884, and *Bacillus bronchiseptica* 4617, which were obtained from Division of Microbiology, Department of Pharmaceutical Technology, Jadavpur University. Clinically used antibacterial agent amoxicillin was employed as the reference material [22]. These strains were grown in Mueller-Hinton agar at 37 °C for 24 h and the suspension was prepared by matching a 0.5 McFarland standard [23]. All the tested compounds were dissolved in 4% DMSO solution along with sterile distilled water making up the 2-mL volume and tested for screening using Agar Dilution [24]. Then, Minimum Inhibitory Concentration was determined as per NCCLS protocol [25] and by INT assay. The drug showing best result against a particular organism is selected from both the sets of drugs, and effect on bacterial growth rate was observed. With same combination of drug and organism from each set, scanning electron microscopy (model: Jeol Jsm-6360) was done to find out the mode of action of drugs as well as to observe the morphological alteration behind drug exposure.

3. Results and discussion

3.1. *Crystal structures of $[Ni(SANEt_2)]_2$ (1) and $[Cu(SANEt_2)]_2$ (2)*

X-ray crystallographic analyses reveal that both **1** and **2** are isomorphous dinuclear species (figures 2 and 3, respectively). In both complexes, the metal centers possess nearly square-planar coordination with deviations of –0.044(1) Å, –0.037(1) Å, 0.089(1) Å, and 0.103(1) Å for Ni1, Ni21, Cu1, and Cu21, respectively, from the ideal planes. S10 and O1 of a ligand bind *trans* to a metal center, with N8 of the same ligand and the phenoxo O21 of another ligand in the other two *trans* sites of the metal center. Phenoxo O1 and O21 are shared by both coordination units. Coordination planes of the two metal units are joined along the line connecting C1, O1, O21, and C21 and are twisted with respect to each other having a torsion angle of 144.03° giving the whole unit an 'X' shape when viewed edge-on. Crystallographic data and refinement parameters are given in table 1.

In **1**, Ni–O distances are 1.88(2)–1.907(2) Å, with Ni1–N8 and Ni2–N28 distances of 1.843(3) Å and 1.842(3) Å. Ni1–S10 and Ni2–S30 distances are 2.136(1) Å and 2.133(1) Å, respectively. The bond angles show no unusual values (table 2).

In **2**, Cu–O distances are 1.936(3)–1.981(3) Å, with Cu1–N8 and Cu2–N28 distances of 1.917(4) Å and 1.934(4) Å, respectively. Cu1–S10 and Cu22–S30 distances are 2.205(1) Å and 2.201(1) Å, respectively. The bond angles are usual for this type of complex (table 3).

In both complexes, all classical hydrogen bonds are intramolecular (table S1, see online supplemental material at http://dx.doi.org/10.1080/00958972.2014.880426).

The supramolecular assemblies of dinuclear units are governed by $\pi\cdots\pi$ and $CH\cdots\pi$ interactions. As depicted in figure 2, the six-member metal chelate rings R4 and R5 and the phenyl rings R6 and R7 are responsible for π-stacking interactions between successive dinuclear units. These π-stacking interactions (table S2) lead to a 1-D chain of the dinuclear

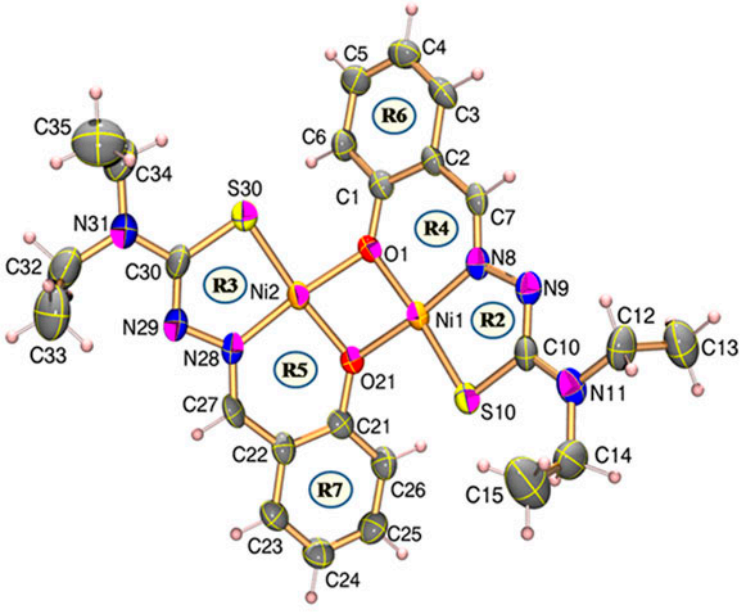

Figure 2. ORTEP diagram (30% ellipsoidal probability) with atom numbering scheme for **1**.

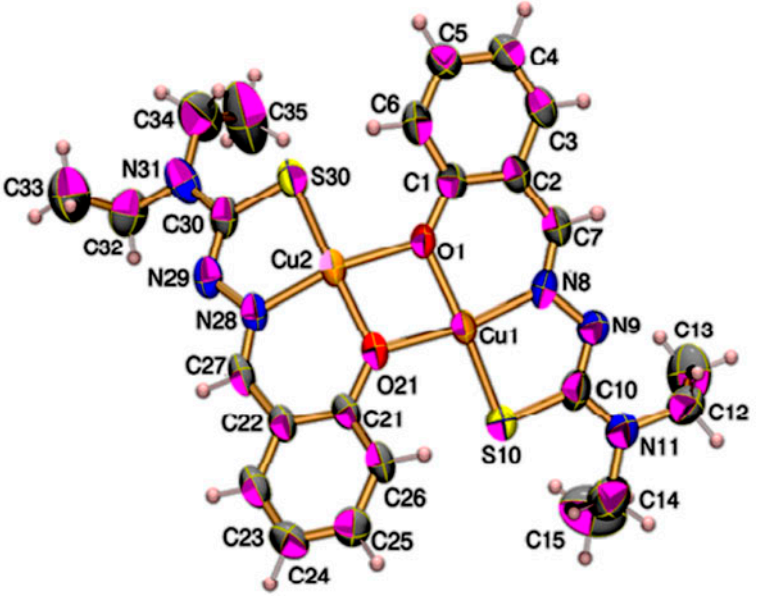

Figure 3. ORTEP diagram (30% ellipsoidal probability) with atom numbering scheme for **2**.

units along the crystallographic *a*-axis (figure 4). Five-member metal chelate rings involving *S* and *N* (*R*2 and *R*3) are also involved in this interaction, forming tubular assembly along the crystallographic *a*-axis through centrosymmetric arrangement of adjacent 'X'-shaped

Table 1. Crystal data and refinement parameters.

Complex	**1**	**2**
Crystal data		
Formula	$Ni_2C_{24}H_{30}N_6O_2S_2$	$Cu_2C_{24}H_{30}N_6O_2S_2$
Formula weight	616.06	625.75
Crystal system	Monoclinic	Monoclinic
Space group	$P2_1/c$ (No. 14)	$P2_1/c$ (No. 14)
a, b, c [Å]	13.342(4), 12.347(3), 16.882(5)	13.432(4), 11.985(3), 17.140(5)
α, β, γ [°]	90, 111.006(6), 90	90, 109.216(8), 90
V [Å^3]	2596.2(13)	2605.5(13)
Z	4	4
D(Calcd) [g/cm^3]	1.576	1.595
μ(MoK$_\alpha$) [mm]	1.646	1.827
F (0 0 0)	1280	1288
Crystal size [mm]	0.10 × 0.10 × 0.10	0.03 × 0.10 × 0.10
Data collection		
Temperature (K)	93	93
Radiation [Å]	MoK$_\alpha$ 0.71075	MoK$_\alpha$ 0.71075
Theta min-max [°]	0.0, 25.4	0.0, 25.4
Data set	−16 : 13; −14 : 13; −15 : 20	−15 : 16; −14 : 10; 20 : 18
Tot., uniq. data, R(int)	15920, 4724, 0.054	15949, 4735, 0.054
Observed data [$I > 0.0\ \sigma(I)$]	3360	3493
Refinement		
Nref, Npar	4724, 325	4735, 325
R, $wR2$, S	0.0462, 0.1051, 1.00	0.0504, 0.1355, 1.07
Max. and av. shift/error	0.01, 0.00	0.02, 0.00
Min. and max. resd. dens. [e/Å^3]	−0.44, 0.56	−0.64, 1.51

Table 2. Selected bond distances and angles (Å, °) for **1**.

Bond distances			
Ni1–S10	2.1360(13)	Ni2–S30	2.1325(12)
Ni1–O1	1.881(2)	Ni2–O1	1.905(2)
Ni1–O21	1.907(2)	Ni2–O21	1.890(2)
Ni1–N8	1.843(3)	Ni2–N28	1.842(3)
Bond angles			
S10–Ni1–O1	174.78(8)	S30–Ni21–O1	98.04(8)
S10–Ni1–O21	98.37(8)	S30–Ni21–O21	173.37(8)
S10–Ni1–N8	87.60(10)	S30–Ni21–N28	87.83(10)
O1–Ni1–O21	77.16(10)	O1–Ni21–O21	76.98(10)
O1–Ni1–N8	96.76(12)	O1–Ni21–N28	174.13(12)
O21–Ni1–N8	173.53(11)	O21–Ni21–N28	97.16(12)
Ni1–S10–C10	95.81(15)	Ni21–S30–C30	95.26(16)
Ni1–O1–C1	127.6(2)	Ni21–O1–C1	130.7(2)
Ni1–O21–C21	130.4(2)	Ni21–O21–C21	126.6(2)
Ni1–N8–N9	122.8(2)	Ni21–N28–N29	122.3(3)
Ni1–N8–C7	123.7(3)	Ni21–N28–C27	123.7(3)
Ni1–O1–Ni21	90.62(10)	Ni1–O21–Ni21	90.30(10)

molecular complexes (figure 4). Terminal –CH_3 groups provide the site for CH$\cdots\pi$ interactions (table S3), through which the tubular units are interconnected (figure 5).

3.2. *DFT structure of [Ni(SANEt$_2$)]$_2$ (1)*

A DFT optimization has been carried out for the Ni(II) complex (figure S1). The calculated optimized geometry is nearly identical to the one observed in the crystal structure. Bond distances are slightly higher in the calculated geometry, Ni–O distances of 1.863 Å and

Table 3. Selected bond distances and angles (Å, °) for **2**.

Bond distances			
Cu1–S10	2.2048(13)	Cu2–S30	2.2005(13)
Cu1–O1	1.939(3)	Cu2–O1	1.981(3)
Cu1–O21	1.967(3)	Cu2–O21	1.936(3)
Cu1–N8	1.917(4)	Cu2–N28	1.934(4)
Bond angles			
S10–Cu1–O1	171.92(11)	S30–Cu2–O1	102.16(9)
S10–Cu1–O21	101.39(8)	S30–Cu2–O21	173.94(11)
S10–Cu1–N8	87.74(10)	S30–Cu2–N28	87.48(10)
O1–Cu1–O21	76.28(11)	O1–Cu2–O21	76.05(11)
O1–Cu1–N8	94.28(13)	O1–Cu2–N28	168.48(12)
O21–Cu1–N8	170.43(12)	O21–Cu2–N28	93.71(13)
Cu1–S10–C10	93.49(17)	Cu2–S30–C30	94.25(17)
Cu1–O1–C1	127.2(3)	Cu2–O1–C1	131.2(3)
Cu1–O21–C21	132.1(3)	Cu2–O21–C21	127.1(3)
Cu1–N8–N9	120.8(3)	Cu2–N28–C27	125.1(3)
Cu1–N8–C7	125.3(3)		
Cu1–O21–Cu2	98.62(13)	Cu1–O1–Cu2	98.04(13)

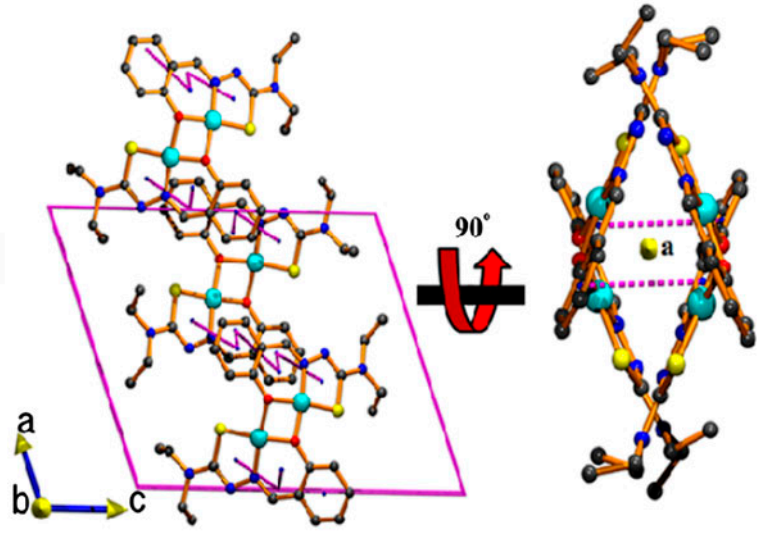

Figure 4. The supramolecular 1-D chain of molecular complexes through $\pi\cdots\pi$ interaction that run along the crystallographic *a*-axis (left) and the tubular view of this chain when seen along the *a*-axis (right). The tube has a rhombic cross-section.

1.891 Å and Ni–N distances 1.837 Å and 1.838 Å. Ni–S distances are identical (2.162 Å). The calculated torsion angle between the two metal coordination planes is 144.03°. The HOMO and LUMO have a gap of 3.546 eV; these frontier orbitals are composed of both metals and ligand orbitals (figure S2).

3.3. *IR spectral studies*

IR spectra of H_2SANEt_2 and its Ni(II) and Cu(II) complexes provide information about the mode of ligand coordination. The band at 1616 cm^{-1} in the ligand spectrum corresponds to

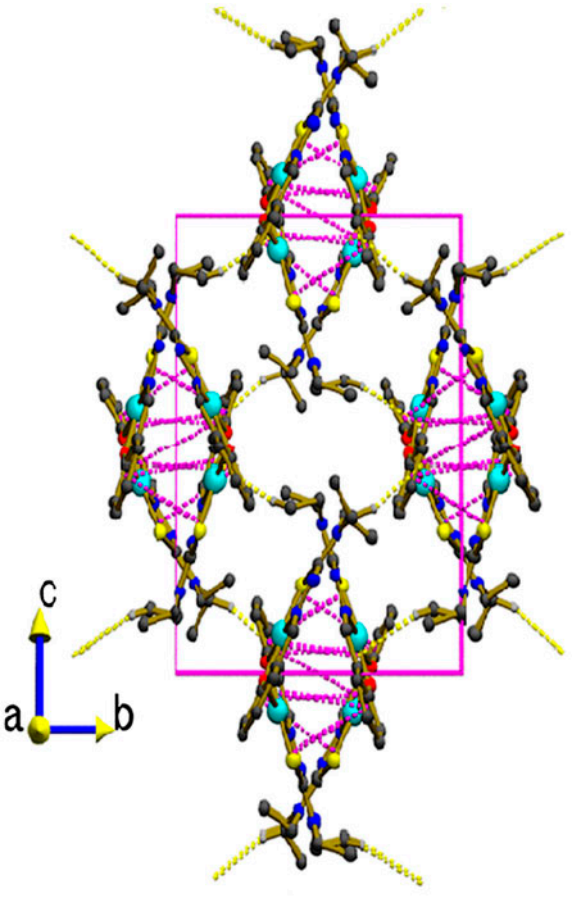

Figure 5. The packing of tubular units through CH···π interaction (shown as yellow dotted lines) in which the terminal –CH_3 groups play a prominent role (see http://dx.doi.org/10.1080/00958972.2014.880426 for color version).

azomethine –CH=N stretch, shifted to 1596 cm^{-1} for Ni(II) and 1593 cm^{-1} for Cu(II) in the metal complexes, indicating that azomethine N participates in bond formation. Another peak at 3361 cm^{-1} due to –NH group of the ligand disappeared in metal complexes, indicating a pi-bond in between the N–C for formation of M–S sigma bond by converting –C=S into –C–S^-. A strong peak at 765 cm^{-1} (–C=S), in ligand, shifted lower in metal complexes supporting this.

3.4. *UV–Vis spectra*

UV–Visible spectra of ligand and complexes in DMSO and in the solid state show that all compounds have same structure in solution and in the solid state. In **1**, a broad absorbance at 22,000 cm^{-1} is due to the $^1A_g \rightarrow {}^1A_{2\,g}$ transition in a square-planar geometry [26]; absorption below 10,000 cm^{-1} also indicates square-planar geometry [27]. Complex **2** showed bands at 30,000 cm^{-1} and 40,000 cm^{-1} corresponding to n–π^* and π–π^* transitions, respectively [28]. The LMCT band, in **2**, appeared around 20,000 cm^{-1} due to Cu–S bonding [29].

3.5. *^{1}H NMR spectrum of H_2SANEt_2*

The ^{1}H NMR spectrum of the free ligand in DMSO-d_6 gives singlets at δ 8.54 (1H) and 11.15 (1H) assigned to salicylaldehyde –CH and thiosemicarbazate –NH, respectively. One-proton singlet at δ 8.54 ppm, ascribed as phenolic –OH proton, indicates the existence of hydrogen-bonded stabilized form of the ligand. The ^{1}H NMR spectrum shows a triplet at δ 6.92 (2H) due to the aromatic protons; the two peaks, a quartet at δ 3.77(4H), and a triplet at 1.19 (6H) are assigned to the two $–CH_2–$ and two $–CH_3$ groups of $–NEt_2$, respectively.

3.6. *Antimicrobial activity*

The ligand and its complexes were active towards antimicrobial effect at MIC concentration 10–400 μg/mL. Ligand is the most active against *V. cholerae* 1363175 with lower MIC concentration 10 μg/mL, whereas **1** is more effective against *S. typhi* 74, *V. cholerae* 1363175, and *S. dysenteriae* 1 at lowest MIC concentration of 10 μg/mL. Complex **2** was active against *S. typhi* 74, *S. dysenteriae* 1, and *S. epidermidis* 12228 at MIC concentration 10 μg/mL (table 4). The compounds are active toward a variety of micro-organisms at different MIC values (table 5). The test drugs are broad spectrum, i.e. effective on both gram-positive and gram-negative organisms, more effective on enteric organisms. As the cell wall architectures were different in the different micro-organisms, there might be a common target of these drugs. By analyzing bacterial growth curve, we conclude that these compounds are bacteriostatic agents. The details of the time-dependent *in vitro* growth curves of different bacteria at MIC values against the complex species are shown in figure 6. The enhanced antimicrobial activity of both complexes may be explained in terms of Overtone's concept of cell permeability [30] and Tweedy's chelation theory [31]. Generally, antimicrobial efficiency decreases in the order cationic > neutral > anionic complex [32], consistent with greater activity of complex over the ligand. The actual process of destruction of bacterial cell has been shown by treating *Sh. sonnie* BCH217 and *Micrococcus* 10240 with ligand

Table 4. Representation of MIC (μg/ml) values of synthetic drugs on tested organisms.

Organisms	Ligand	Complex **1**	Complex **2**	AM*
S. typhi 74	–	10	10	25
E. coli 55/10HD	–	50	–	1
M. luteus 9341	–	400	–	5
S. aureus ML191	–	50	25	5
K. pneumoniae 714	400	50	25	100
Pseudomonas AMRI 100	–	400	–	100
V. cholerae 1363175	10	10	10	25
Sh. sonnei BCH217	200	400	–	50
P. vulgaris 24	400	–	–	256
S. faecalis 52	400	–	–	5
S. dysenteriae 1	200	10	10	1
B. cereus 11778	400	50	400	25
P. aureginosa 25619	400	–	–	100
Micrococcus sp. 10240	400	50	100	25
B. subtilis 6633	–	100	–	25
B. pumilus 14884	400	100	–	50
B. bronchiseptica 4617	100	100	–	50
S. epidermidis 12228	–	50	10	5

AM* = amoxicillin, which is used as a standard drug.
"–" represents no antimicrobial activity.

Table 5. Zone diameter of MIC (mm) values of synthetic drugs on tested organisms.

Organisms	Ligand	Complex **1**	Complex **2**	AM*
S. typhi 74	–	6.0 ± 0.2	8.0 ± 0.1	8.5 ± 0.5
E. coli 55/10HD	–	8.0 ± 0.2	–	13.3 ± 0.9
M. luteus 9341	–	7.0 ± 0.7	–	7.0 ± 0.2
S. aureus ML191	–	7.2 ± 0.7	6.0 ± 0	15.5 ± 0.9
K. pneumoniae 714	6.4 ± 0.1	8.0 ± 0.2	8.0 ± 0.2	9.0 ± 0.9
Pseudomonas AMRI 100	–	–	–	9.0 ± 0.6
V. cholerae 1363175	7.0 ± 0.2	7.0 ± 0.7	6.2 ± 0.1	7.5 ± 0.5
Sh. sonnei BCH217	7.0 ± 0.1	6.2 ± 0.1	–	8.6 ± 0.1
P. vulgaris 24	7.5 ± 0.1	–	–	11 ± 4
S. faecalis 52	6.1 ± 0.1	–	–	9.2 ± 0.3
S. dysenteriae 1	6.0 ± 0.1	7.2 ± 0.2	6.0 ± 0.2	9.5 ± 0.5
B. cereus 11778	–	6.0 ± 0	6.0 ± 0	12.0 ± 0.2
P. aeruginosa 25619	8.2 ± 0.2	–	–	9.5 ± 0.6
Micrococcus sp. 10240	6.1 ± 0.1	8.0 ± 0.2	6.0 ± 0.2	7.8 ± 0.8
B. subtilis 6633	–	6.4 ± 0	–	12.7 ± 0.2
B. pumilus 14884	7.0 ± 0.1	7.1 ± 0.2	–	11.6 ± 0.6
B. bronchiseptica 4617	6.4 ± 0.1	6.6 ± 0.1	–	
S. epidermidis 12228	–	6.5 ± 0	6.5 ± 0.1	13.0 ± 0.4

AM* = amoxicillin, which is used as a standard drug.
"–" represents no zone of inhibition of drugs.

and **1**, respectively, as referenced under SEM. Ligand made the cell fragile and subsequently made leakage of cytoplasm in *Sh. sonnie* BCH217 (figure 7); **1** caused swelling of *Micrococcus* 10240 cell and deformation of structure by increasing cell permeability (figure 8).

3.7. *Magnetic property*

The magnetic measurements of **2** were performed with a SQUID magnetometer (MPMS-7 Quantum Design) from 2 to 300 K with an applied field of 1 Tesla on a powdered microcrystalline sample. The magnetic susceptibility data of χT *versus* T (χ for two copper(II) ions) of **2** are shown in figure 9 and the parameters are shown in table 6. All experimental magnetic data were corrected for the underlying diamagnetism of the sample holder and of the constituent atoms (Pascal's tables). Magnetic susceptibility could be fitted by the least square method with the classic Bleaney–Bowers equation [33]. For the spin Hamiltonian simulations of the data, the routine JulX was used. The simulation was obtained by using the Hamilton:

$$\hat{H} = -2\sum_{i<j} J_{i,j}\hat{S}_i\hat{S}_j$$

The χT at room temperature is 0.15 $cm^3\ K\ M^{-1}$, which lies far below the value of 0.75 $cm^3\ K\ M^{-1}$ expected for two uncoupled spins with $S_1 = S_2 = 0.5$. The χT value decreases rapidly with decreasing temperature reaching a constant value close to 0 $cm^3\ K\ M^{-1}$ at ~100 K and follows the Curie−Weiss law with Weiss constant $\theta = 0$ K. This magnetic behavior is generally observed for complexes that possess a strong intracomplex antiferromagnetic interaction [34, 35]. The antiferromagnetic coupling for the complex is $J_{12} = -299$ cm^{-1}, $g_1 = g_2 = 2.00$ and a paramagnetic impurity of 2.2% with a spin of S (PI) = 1 and a

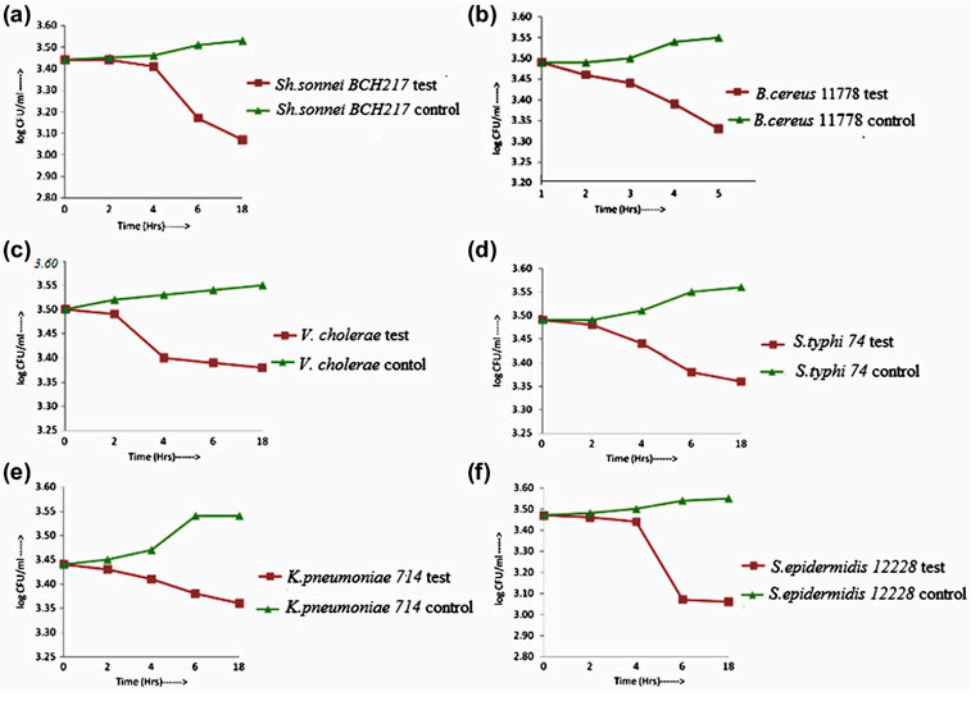

Figure 6. Time-dependent *in vitro* growth curves at MIC values of (a) *Sh. sonnei* BCH217 against ligand; (b) *B. cereus* 11778 against ligand; (c) *V. cholerae* 1363175 against complex **1**; (d) *S. typhi* 74 against **1**; (e) *K. pneumoniae* 714 against complex **2**; and (f) *S. epidermidis* 12228 against **2**.

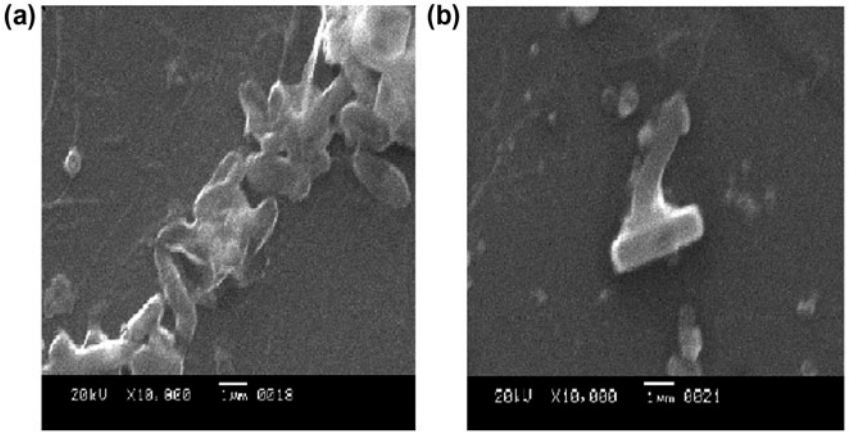

Figure 7. SEM micrographs of *Sh. sonnei* BCH217: before [figure 7(a)] and after [figure 7(b)] treating with ligand.

Theta–Weiss temperature of 0 K of the impurity. TIP is the temperature-independent paramagnetism. Thus, the J value here shows a strong antiferromagnetic interaction between two copper(II) ions. The dominant exchange pathway, through the two oxygen

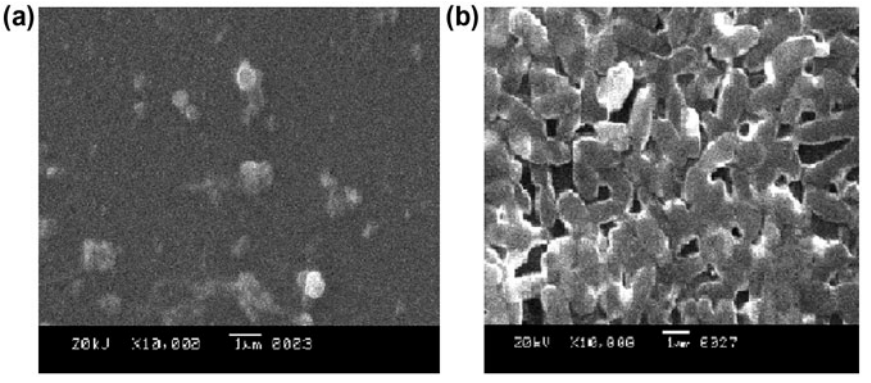

Figure 8. Representative SEM micrographs of *Micrococcus* 10240: before [figure 8(a)] and after [figure 8(b)] treating with **1**.

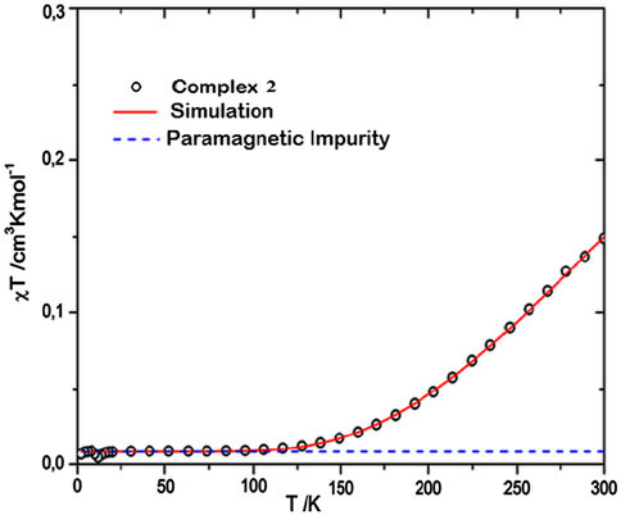

Figure 9. The magnetic susceptibility data of χT *vs*. T plot of **2**.

Table 6. Magnetic parameters for **2**.

S_1	S_2	J_{12}/cm^{-1}	g_1	g_2	TIP/1e-6emu	Imp/%	Spin of PI	Theta–Weiss PI/K
0.5	0.5	−299.233	2.0	2.0	50	2.2	1	1

bridges, involves interaction of two copper $d_{x^2-y^2}$ orbitals and an 's' and a 'p' orbital on the oxygen with predominantly σ overlap. Out of plane distortions at the copper centers of **2** may be due to some reduction of σ overlap and as well as exchange, but the effect on the exchange is small. Because of the proximity of the two metal centers in the $N_2S_2O_2$ framework, this magnetic behavior may be assigned as an 'intramolecular antiferromagnetic exchange interaction' propagated by the endogenous bridging oxygens [36].

4. Conclusion

The present communication provides a general and effective method for the synthesis of salicylaldehyde-N(4)-diethylthiosemicarbazone (H_2SANEt_2) and its Ni(II) and Cu(II) complexes. The complexes are neutral, oxygen-bridged dinuclear species, and crystallize in monoclinic crystal system with nearly square-planar geometries around the metal. All the compounds show potential antimicrobial actions against pathogenic bacteria. The ligand is active against *V. cholerae* 1363175, but coordination of the thiosemicarbazone to nickel(II) resulted in enhancement of activity against *S. typhi* 74 and *S. dysenteriae* 1. Coordination to copper(II) resulted in enhancement of activity against almost all the studied micro-organisms. The compounds are effective against both gram-positive and gram-negative organisms. Hence, complexation of the thiosemicarbazone ligand with the metal enhances the antimicrobial activities, as observed in similar type of complexes [37, 38]. Complex **2** shows strong antiferromagnetic interaction between two Cu(II) centers coupled via the bridging phenoxo O.

Supplementary material

Crystallographic data for the structures reported here have been deposited with the Cambridge Crystallographic Data Center, CCDC Nos. 903324 and 903325. Copies of this information may be obtained free of charge from the Director, CCDC, 12 Union Road, Cambridge, CB2 1EZ, UK (Fax: +44-1223-336-033); E-mail: deposit@ccdc.cam.ac.uk or http://www.ccdc.cam.ac.uk.

Acknowledgments

One of us (Rajesh Pradhan) is thankful to University of Kalyani for providing financial support in the form of University Research fellowship. The financial support received from the DST-PURSE program, University of Kalyani, is thankfully acknowledged.

References

[1] T.A. Yousef, G.M. Abu El-Reash, O.A. El-Gammal, R.A. Bedier. *J. Mol. Struct.*, **1029**, 149 (2012).
[2] M. Hakimi, R. Takjoo, V. Erfaniyan, E. Schuh, F. Mohr. *Transit. Metal Chem.*, **35**, 959 (2010).
[3] Y. Kang, N. Yang, S.O. Kang, J. Ko. *Organometallics*, **16**, 5522 (1997).
[4] D.X. West, J.K. Swearingen, J. Valdés-Martínez, S. Hernández-Ortega, A.K. El-Sawaf, F. van Meurs, A. Castiñeiras, I. Garcia, E. Bermejo. *Polyhedron*, **18**, 2919 (1999).
[5] P. Tarasconi, S. Capacchi, G. Pelosi, M. Cornia, R. Albertini, A. Bonati, P.P. Dall'Aglio, P. Lunghi, S. Pinelli. *Bioorg. Med. Chem.*, **8**, 157 (2000).
[6] A. Kumar, Usha, S. Chandra. *Synth. React. Inorg. Met. Org. Chem.*, **23**, 671 (1993).
[7] L.J. Ackerman, P.E. Fanwick, M.A. Green, E. John, W.E. Running, J.K. Swearingen, J.W. Webb, D.X. West. *Polyhedron*, **18**, 2759 (1999).
[8] J. Straiat, P. Kovarikova, J. Klimes, D.S. Kalinowski, D.R. Richardson. *Anal. Bioanal. Chem.*, **39**, 7161 (2010).
[9] U.P. Singh, R.K. Singh, H.R. Bhat, Y.P. Subhashchandra, V. Kumar, M.K. Kumawat, P. Gahtori. *Med. Chem. Res.*, **20**, 1603 (2011).
[10] M.C. Rodríguez-Argüelles, P. Tourón-Touceda, R. Cao, A.M. García-Deibe, P. Pelagatti, C. Pelizzi, F. Zani. *J. Inorg. Biochem.*, **103**, 35 (2009).

[11] M. Devereux, D.O. Shea, A. Kellett, M. McCann, M. Walsh, D. Egan, C. Deegan, K. Kędziora, G. Rosair, H. Müller-Bunz. *J. Inorg. Biochem.*, **101**, 881 (2007).
[12] R. Prabhakaran, P. Kalaivani, R. Huang, P. Poornima, V. Vijaya Padma, F. Dallemer, K. Natarajan. *J. Biol. Inorg. Chem.*, **18**, 233 (2013).
[13] E. Labisbal, K.D. Haslow, A. Sousa-Pedrares, J. Valdés-Martínez, S. Hernández-Ortega, D.X. West. *Polyhedron*, **22**, 2831 (2003).
[14] P. Roy, M. Nandi, M. Manassero, M. Riccó, M. Mazzani, A. Bhaumik, P. Banerjee. *Dalton Trans.*, **43**, 9543 (2009).
[15] N.C. Saha, C. Biswas, A. Ghorai, U. Ghosh, S.K. Seth, T. Kar. *Polyhedron*, **34**, 1 (2012).
[16] L.F. Audrieth, E.S. Scott, P.S. Kippur. *J. Org. Chem.*, **19**, 733 (1954).
[17] J.P. Scovill. *Phosphorus, Sulfur Silicon Relat. Elem.*, **60**, 15 (1991).
[18] G.M. Sheldrick. *SHELX 97, Program for Refinement of Crystal Structure*, University of Göttingen, Germany (1997).
[19] D.T. Cromer, J.T. Weber. *International Tables for X-ray Crystallography*, Table 2.2A, Vol. IV, The Kynoch Press, Birmingham (1994).
[20] J.A. Ibers, W.C. Hamilton. *Acta Crystallogr.*, **17**, 781 (1964).
[21] M.W. Schmidt, K.K. Baldridge, J.A. Boatz, S.T. Elbert, M.S. Gordon, J.H. Jensen, S. Koseki, N. Matsunaga, K.A. Nguyen, S.J. Su, T.L. Windus, M. Dupuis, J.A. Montgomery. *J. Comput. Chem.*, **14**, 1347 (1993).
[22] K.B. Sahu, S. Ghosh, M. Banerjee, A. Maity, S. Mondal, R. Paira, P. Saha, S. Naskar, A. Hazra, S. Banerjee, A. Samanta, N.B. Mondal. *Med. Chem. Res.*, **22**, 94 (2013).
[23] J. McFarland. *JAMA*, **14**, 1176 (1907).
[24] M.K. Paira, T.K. Mondal, D. Ojha, A.M.Z. Slawin, E.R.T. Tiekink, A. Samanta, C. Sinha. *Inorg. Chim. Acta*, **370**, 175 (2011).
[25] National Committee for Clinical Laboratory Standards (NCCLS). *Approved Standard M7 A3*, 3rd Edn., NCCLS, Villanova, (1993).
[26] M. Nashwa, E. Metwally, I.M. Gabr, A.A. El-Asmy. *Transit. Metal Chem.*, **31**, 71 (2006).
[27] A.B.P. Lever. *Inorganic Electronic Structure and Spectroscopy*, 1st Edn, p. 343, Elsevier, Amsterdam (1968).
[28] J.R. Gujarathi, N.S. Pawar, R.S. Bendre. *Der Pharma Chem.*, **5**, 111 (2013).
[29] O.A. El-Gammal, G.M. Abu El-Reash, S.E. Ghazy, T. Yousef. *J. Coord. Chem.*, **65**, 1655 (2012).
[30] N. Raman, A. Kulandaisamy, K. Jayasubramanian. *Pol. J. Chem.*, **76**, 1085 (2002).
[31] B.G. Tweedy. *Phytopathology*, **55**, 910 (1964).
[32] E.K. Efthimiadou, M.E. Katsarou, A. Karaliota, G. Psomas. *J. Inorg. Biochem.*, **102**, 910 (2008).
[33] L. Wu, J. Wang, C. Zhu, Y. Lin, L. Chen, J. Fan, H. Zhang. *Sci. China Chem.*, **53**, 1255 (2010).
[34] M. Sutradhar, T. Roy Barman, J. Klanke, M.G.B. Drew, E. Rentschler. *Polyhedron*, **53**, 48 (2013).
[35] B.K. Tripuramallu, S. Mukherjee, S.K. Das. *Cryst. Growth Des.*, **12**, 5579 (2012).
[36] A.D. Naik, S.M. Annigeri, U.B. Gangadharmath, V.K. Revankar, V.B. Mahale. *J. Inclusion Phenom. Macrocyclic Chem.*, **43**, 291 (2002).
[37] U. El-Ayaan. *J. Coord. Chem.*, **65**, 629 (2012).
[38] J.G. da Silva, C.C.H. Perdigão, N.L. Speziali, H. Beraldo. *J. Coord. Chem.*, **66**, 385 (2013).